Late Pliocene Cordilleran Ice Sheet development with warm Northeast Pacific sea surface temperatures

Maria Luisa Sánchez-Montes[1], Erin L. McClymont[1], Jeremy M. Lloyd[1], Juliane Müller[2], Ellen A. Cowan[3] and Coralie Zorzi[4].

[1] Geography Department, Durham University, Durham, DH1 3LE, UK.
[2] Alfred Wegener Institute, Helmholtz Centre for Polar and Marine Research, Bremerhaven, 27568, Germany.
[3] Department of Geological and Environmental Sciences, Appalachian State University, North Carolina, 28608, USA.
[4] GEOTOP, Université du Québec à Montréal, Montreal, H3C 3P8, Canada.

Correspondence to: Maria Luisa Sánchez Montes (m.l.sanchez-montes@durham.ac.uk)

Abstract. The initiation and evolution of the Cordilleran Ice Sheet is relatively poorly constrained. International Ocean Discovery Program (IODP) Expedition 341 recovered marine sediments at Site U1417 in the Gulf of Alaska (GOA). Here we present alkenone-derived sea surface temperature (SST) analyses alongside ice rafted debris (IRD), terrigenous and marine organic matter inputs to the GOA through the late Pliocene and early Pleistocene. The first IRD contribution from tidewater glaciers in southwest Alaska is recorded at 2.9 Ma, indicating that the Cordilleran ice sheet extent increased in the late Pliocene. A higher occurrence of IRD and higher sedimentation rates in the GOA during the early Pleistocene, at 2.5 Ma, occur in synchrony with SSTs warming on the order of 1°C relative to the Pliocene. All records show a high degree of variability in the early Pleistocene, indicating highly efficient ocean-climate-ice interactions through warm SST-ocean evaporation-orographic precipitation-ice growth mechanisms. A climatic shift towards ocean circulation in the subarctic Pacific similar to the pattern observed during negative Pacific Decadal Oscillation (PDO) conditions today appears to be a necessary pre-requisite to develop the Cordilleran glaciation and increase moisture supply to the subarctic Pacific. The drop in atmospheric CO_2 concentrations since 2.8 Ma is suggested as one of the main forcing mechanisms driving the Cordilleran glaciation.

1 Introduction

During the Neogene, the global climate transitioned from relatively warm to cooler conditions that enabled the development of ice masses in both hemispheres (Zachos *et al*., 2001a). The Mid-Piacenzian Warm Period (MPWP, 3.3-3.0 Ma) interrupts this cooling trend, with global temperatures around 2-3 °C above pre-industrial levels (Jansen *et al*., 2007; Haywood *et al*., 2004), and more intense warming at higher latitudes (Haywood *et al*., 2013; Dolan *et al*., 2015). The MPWP has been suggested as a potential analogue for the 21st century climate due to the atmospheric CO_2 concentrations (400 ppmv) and largely equivalent continental configurations relative to the present (Salzmann *et al*., 2011; Raymo *et al*., 1996, Jansen *et al*., 2007). Overall, the mid-Pliocene ice masses were smaller than today (Dolan *et al*., 2011). However, the marine isotope stage (MIS) M2 (~3.3-3.26 Ma) event is characterised by a dramatic cooling in the Atlantic Ocean and is considered to be an unsuccessful

attempt at a glaciation (De Schepper *et al.*, 2013). The later onset (oNHG) or intensification (iNHG) of the Northern Hemisphere Glaciation is marked by the expansion of the Laurentide, Greenland and Scandinavian ice sheets around 2.5 Ma indicated by ice rafted debris (IRD) records from the North Atlantic Ocean (i.e. Shackleton *et al.*, 1984) and the advance of the Cordilleran Ice Sheet at 2.7 Ma inferred from a terrestrial record (Hidy *et al.*, 2013). It is still debated whether climatic or tectonic forcing was the main driver of the North Hemisphere Glaciation (NHG) (Haug *et al.*, 2005), as it cannot be explained solely by changes in isolation (Lunt *et al.*, 2008). The decrease in atmospheric CO_2 concentrations and radiative forcing at 2.8 Ma has been identified as a potential mechanism for climate cooling of the oNHG (Seki *et al.*, 2010; Martínez-Botí *et al.*, 2015). However, the timing of the oNHG varies between locations based on IRD delivery, and at some locations the NHG has been set as far back as 3.5 Ma (Nordic Seas, Mudelsee and Raymo, 2005). Alternative proposals for the oNHG suggest that orogenic changes could have led to an increase in heat transport to the North Atlantic region during the Pliocene potentially increasing precipitation in higher latitudes promoting glacial development during the Plio-Pleistocene transition (Sarnthein *et al*, 2013; Haug *et al.*, 2005; Bringham-Grette *et al.,* 2013; Fedorov *et al.,* 2013; Lawrence *et al.,* 2010).

It remains unclear whether the Cordilleran Ice Sheet of North America expanded across the oNHG, although enhanced delivery of terrigenous sediments to the Gulf of Alaska (GOA; Northeast Pacific Ocean) since 2.7 Ma has been interpreted as evidence for ice sheet growth (Gulick *et al.*, 2014). The sediments of the Gulf of Alaska (GOA) record Cordilleran glaciation in the St. Elias Mountains, at present the highest coastal mountain range in the world (Enkelmann *et al.*, 2015). It has been proposed that the uplift of the St. Elias Range from early Pliocene to early Pleistocene led to an increase in orographic precipitation and subsequent increase in sedimentation rates in the GOA (Enkelmann *et al.*, 2015). Mountain glaciation may have developed in the St Elias mountains as early as 5.5 Ma (Reece *et al.*, 2011), ultimately developing tidewater glaciers, with the high erosion pathway shifting to the southern St Elias Range at 2.6 Ma (Enkelmann *et al.*, 2015). Rather than a tectonic control on Cordilleran glaciation, an alternative explanation could be the reduced radiative forcing and climate cooling associated with the decline in CO_2 at 2.8 Ma. However, it is difficult to resolve these hypotheses in the absence of high resolution data for both ice sheet extent and climate from the GOA. Despite the global drop in atmospheric CO_2 at 2.8 Ma, it remains unclear whether the Cordilleran Ice Sheet also expanded.

Here, we present a new multiproxy data set obtained from IODP core site U1417 (56° 57.58' N, 147° 6.58' W, water depth 4218 m; Fig. 1) in the GOA. The core site allows examination of the land-ocean interactions associated with advance and retreat phases of the Cordilleran Ice Sheet across the Pliocene-Pleistocene transition, in the context of mountain uplift. The sediments were collected during IODP Expedition 341 (Jaeger *et al.,* 2014) and were analysed to reconstruct sea surface conditions by means of alkenone and IRD data covering the time interval from 4 to 1.7 Ma years ago. Terrestrial organic matter input to Site U1417 is assessed through the abundance of long-chain *n*-alkanes and palynological analysis.

2 Study area

2.1 The Gulf of Alaska (GOA)

The GOA extends from the Alaska Peninsula in the west to the Alexander Archipelago in the east (Hogan, 2013), delimited by the Bering Sea on the west and the Alaska coast in the north and east, which is, in turn, bounded to the north by the Pacific Mountain System (Molnia, 2008). The south of the GOA connects with the North Pacific Ocean (Fig. 1). Glaciers cover 20% of the Gulf of Alaska watershed (Spies, 2007), and the major rivers draining the St. Elias and Chugach mountains towards the GOA (the Alsek River and the Copper River), are fed by meltwater discharge which peaks in August (Weingartner, 2007). The GOA mean annual freshwater discharge derives from high precipitation, runoff and snow melt from watersheds along the SE Alaskan coast (Spies, 2007). High precipitation is due in part to the proximity of the North Pacific Ocean, as a source of moisture, and the high topography of the Pacific Mountain System driving orographic precipitation.
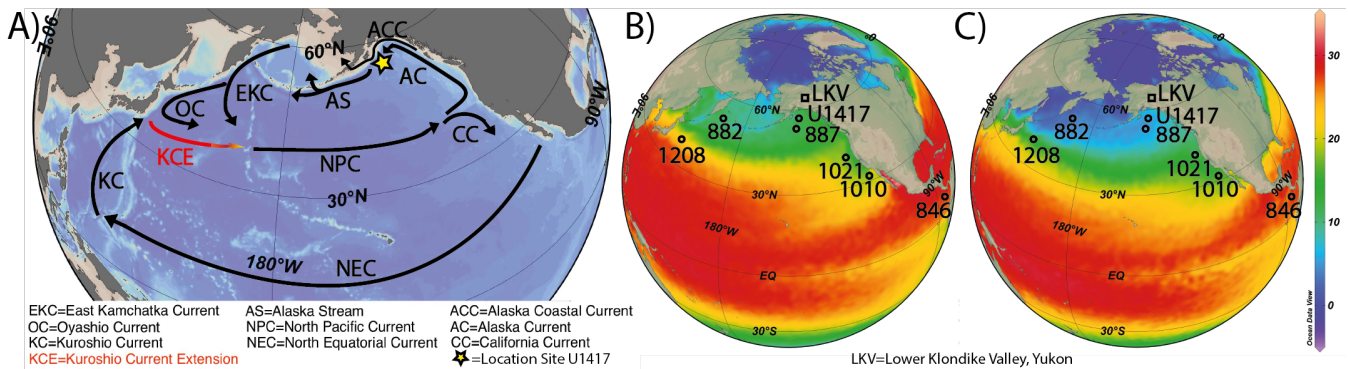
Figure 1: Map of modern ocean circulation and SSTs. a) Modern North Pacific Ocean circulation, b) September c) and December 1955-2013 SST average centred in the North Pacific Ocean (NOAA WOA13, Locarnini *et al.*, 2013) and core and sample sites discussed in this study. Map made using Ocean Data View (Schlitzer, 2018).

The Alaskan Coastal Current (ACC) flows anti-clockwise along the GOA coastline and westward to the Bering Sea (Fig. 1a), and its properties are dominated by nutrient and meltwater supply from the coastal Alaskan glaciers (Spies, 2007). Further offshore, the Alaska Current (AC) also flows anti-clockwise, controlled in strength by the Alaska Gyre (Kato *et al.*, 2016) (Fig. 1a). The location of Site U1417 rests under the modern influence of the AC (Fig. 1). The Alaskan Gyre is, in turn, influenced by atmospheric circulation via the Aleutian Low (AL) and the Pacific High Pressure Systems, which are coupled in an annual cycle. High pressures dominate during the summer season and low pressures dominate during autumn to spring (Hogan, 2013), when the AL also migrates eastward across the North Pacific Ocean, becoming most intense when located in the GOA during winter (Pickart *et al.,* 2009). The coast of Alaska receives high winter precipitation because of the AL winter position and strength (Rodinov *et al.,* 2007) and Alaska's high topography which drives orographic precipitation. The GOA locally receives annual precipitation of ~800 cm (Powell and Molnia, 1989). During summer, the AL is less intense and almost disappears when it is located in the Bering Sea. A weaker AL is translated into reduced precipitation over the GOA.

A strong winter AL also creates a strong zonal SST gradient in the North Pacific Ocean (Fig. 1b). During winter, the ocean responds to a more intense AL through southward movement of the cold Arctic waters, and northward flow of mid-latitude warm waters into the Gulf of Alaska through the AC. During the summer migration of the AL northwards, the GOA registers

higher SSTs due to higher insolation on the North Pacific Ocean, and as the zonal SST gradient is reduced, the storms diminish (Pickart *et al.,* 2009) (Fig. 1c).

3 Material and Methods

3.1 Age model and sedimentation rates

5   The shipboard age model was calculated using magnetostratigraphy (Jaeger *et al*., 2014, Fig. S1-3). The recovery of the Pliocene-early Pleistocene sediments averaged 70 % (Expedition 341 Scientists, 2014), with a number of core breaks in the record. Poor carbonate preservation across the Pliocene and early Pleistocene prevents the production of a higher resolution stable isotope stratigraphy. The shipboard depth models place all discrete core biscuits to the upper depth range of each core, and a continuous core break below; it is possible that the biscuits were originally distributed through the core barrel before

10   recovery on the ship. We have converted the depth scale of our data sets to assume an even distribution of core biscuits and core breaks (Fig. S1), converted these depths to age and interpolated the ages of the samples between core top and bottom (Fig. 2 and Figs. S1-S3). The magnetostratigraphy ages were similar between the shipboard and new age model; The Gauss/Matuyama magnetic reversal (2.581 ±0.02 Ma and 330.76 ±1 m CCSF-A) was well constrained in multiple holes to provide an important age control point for this study (Fig. S1). The shipboard age model sedimentation rates show a marked

15   but temporary increase between 2.5-2.0 Ma, which has been attributed to the first major erosion of the landscape by expansion of the Cordilleran Ice Sheet (Gulick *et al*., 2014). Our new sedimentation rates detail a two-step increase from 2.5-2.4 and from 2.4-2.0 Ma (Fig. S3).

3.2 Biomarkers

  A total of 119 biomarker samples between 4 and 1.7 Ma were analysed for biomarkers, which corresponds to an average

20   sampling resolution of 19 kyr. Microwave lipid biomarker extraction was carried out following the method of Kornilova and Rosell-Melé (2003). The total lipid extract was separated into 4 fractions by silica column chromatography, through sequential elution with Hexane (3 ml), Hexane: Dichloromethane (9:1) (1.5 ml), Dichloromethane (5.5 ml) and Ethylacetate:Hexane (20:80) (4 columns) to generate: *n* -alkanes, aromatics, ketone and polar fractions.

  The *n*-alkane fraction was analysed by different sets of gas chromatography (GC) configurations for compound quantification

25   and identification. A Thermo Scientific Trace 1310 gas chromatograph was fitted with flame ionization detector (GC-FID) and a split-splitless injector. Compressed air is set as the air flow, helium (He) is set as the carrier flow, nitrogen (N) as a make-up flow and hydrogen (H) helps with ignition. The oven temperature was set at 70 °C for 2 min, then increased to 170 °C at 12 °C min^{-1}, then increased to 310 °C at 6.0 °C min^{-1}, then held at 310 °C for 35 min. *N*-alkanes were separated using a 60 m x 0.25 mm i.d., Restek RXi-5ms column. (0.25 μm 5% diphenyl-95% dimethyl polysiloxane coating). Compound

30   identification was confirmed using a Thermo Scientific Trace 1310 gas chromatography mass spectrometer (GC-MS), equipped with a programmable temperature vaporizer (PTV) injector. He was used as a carrier flow. The oven temperature

program was set at 60 °C during 2 min and then raised at 12 °C min^{-1} until reaching 150 °C and then raised again to 310 °C at 6 °C min^{-1} and held for 25 min. Compounds were quantified with reference to internal standards (5α-cholestane) and normalised to the original extracted dry weight of sediment, and to sedimentation rate changes by calculating the mass accumulation rate (MAR). The ratio of higher land-plant derived long-chain *n*-alkanes against aquatic sourced short-chain *n*-alkanes (TAR) (Eq. (1); Cranwell, 1973) and the carbon preference index (CPI) (Eq. (2); Bray and Evans, 1961) were calculated using GC-FID peak areas of the respective compounds:

$$\text{TAR} = \frac{[C27]+[C29]+[C31]}{[C15]+[C17]+[C19]} \tag{1}$$

$$\text{CPI} = \frac{\frac{[C25-33(odd)]}{[C24-32(even)]} + \frac{[C25-33(odd)]}{[C26-34(even)]}}{2} \tag{2}$$

Terrigenous and aquatic organic matter sources increase during the early Pleistocene in comparison with the late Pliocene. High TAR values can be indicative of relative increases in terrigenous organic matter transported to the ocean and/or to relative decreases in aquatic microorganism production. The opposite could explain low TAR values. To disentangle the old organic matter contamination from the fresh signal, we include the CPI index (Bray and Evans, 1961). High CPI values indicate a fresher or relatively newly produced organic matter transported to the ocean. CPI close to 1 indicate mature or old organic matter sources, such as coal or oil deposits, eroded to the ocean. This distinction may be important in the GOA, where the onshore bedrock includes units with high contents of terrigenous organic matter (e.g. the Yakutat Terrain, Childress, 2016; Walinsky *et al.*, 2009).

Alkenones (ketone fractions) were quantified by a GC coupled with chemical ionisation mass spectrometry (GC-CIMS), adapted from the method of (Rosell-Melé *et al.*, 1995). Analyses were performed using a Trace Ultra gas chromatograph directly coupled to a Thermo DSQ single quadrupole mass spectrometer, fitted with a programmed temperature vaporising (PTV) injector. 1.2 ml of sample is injected. Alkenones were separated using a 30 m x 0.25 mm i.d., Restek RXi-5ms column (0.25 μm 5% diphenyl-95% dimethyl polysiloxane coating). Helium was employed as the carrier gas (2 ml min^{-1}). The injector was held at 120 °C and splitless mode (1.2 min) during injection, and then immediately temperature programmed from 120 °C to 310 °C at 10 °C s^{-1}, then held for 0.6 min. The oven was programmed to hold at 175 °C for 1.7 min, then increased to 310 °C at 11 min^{-1}, and held at from 310 °C for 12 min. The mass spectrometer was operated in positive chemical ionisation mode (PICI), using high-purity anhydrous ammonia (N6.0, BOC) introduced to the ion source through the CI gas inlet. Selected ion monitoring was performed, targeting the 8 ions corresponding to the [M + NH4]$^{+}$ adducts of the target C_{37} and C_{38} alkenones and the internal standard (2-nonadecanone), each with a selected ion monitoring (SIM) width of 1 m z^{-1} and a dwell time of 30 min. The target m z^{-1} were: 300 (2-nonadecanone), 544 ($C_{37:4}$), 546 ($C_{37:3}$), 548 ($C_{37:2}$), as detailed by (Rosell-Melé *et al.*, 1995). The alkenone U^{K}_{37}' index has been converted into SST according to the core-top to annual mean SST correlation constructed with samples spanning 60° S to 60° N (including from the Pacific Ocean), which accuracy is constrained by an standard error of ±1.5 °C (Eq. (3); Müller *et al.*, 1998). The more recently developed BAYSPLINE SST calibration (Tierney and Tingley, 2018) provides similar SST estimates in the northern latitudes to previous calibrations. The seasonality in the

alkenone production has been evidenced in the North Pacific (Tierney and Tingley, 2018). The SST calibration of Prahl *et al*. (1988) (Eq. (4)), which includes the $C_{37:4}$ alkenone, is also displayed here for comparison, as some concerns have arisen with the use of the U^{K}_{37}' index in samples with high $C_{37:4}$ in the Nordic Seas (Bendle *et al*., 2005). The standard error of Prahl *et al*. (1988) (Eq. (4)) is ±1.0 °C. We identify samples with high $C_{37:4}$ by presenting the percentage of $C_{37:4}$ relative to the other C_{37} alkenones, $\%C_{37:4}$ (Bendle and Rosell-Melé, 2004) (Eq. (5)). The $\%C_{37:4}$ represents fresher and cooler surface water characteristics (Bendle *et al*., 2005). In the Nordic Seas this has been linked to subpolar and polar water masses (Bendle *et al.,* 2005), whereas elsewhere in the North Atlantic it has been linked to freshwater inputs (e.g. during Heinrich events, Martrat *et al.*, 2007). In the subarctic Pacific, the $\%C_{37:4}$ proxy has been less well studied (McClymont *et al*., 2008), but high $\%C_{37:4}$ is also proposed to reflect cooler and fresher water masses (Harada *et al*., 2006).

$$U^{K}_{37}{}' = \frac{[C_{37:2}]}{[C_{37:2}]+[C_{37:3}]} = 0.033SST - 0.044 \tag{3}$$

$$U^{K}_{37} = \frac{[C_{37:2}]-[C_{37:4}]}{[C_{37:2}]+[C_{37:3}]+[C_{37:4}]} = 0.040SST - 0.104 \tag{4}$$

$$\%C_{37:4} = \frac{[C_{37:4}]}{[C_{37:2}]+[C_{37:3}]+[C_{37:4}]}*100 \tag{5}$$

3.3 IRD

IRD were quantified by weighing the coarse sand fraction (250 μm^{-2} mm) following the method of Krissek (1995). Coarse sand was separated from 10 cm^3 samples by wet sieving after air drying and rinsing with distilled water to remove salts. Each sand sample was examined with a binocular microscope to estimate the volume of terrigenous ice-rafted sediment (in volume percent) in order to exclude biogenic components and burrow fills of manganese and pyrite, which do not have an ice-rafted origin. The mass accumulation rate of IRD (in grams per cm^2 kyr^{-1}) was calculated as in Eq. (6):

$$IRD\,MAR = CS\% * IRD\% * DBD * LSR \tag{6}$$

where CS% is the coarse sand abundance (multiplied as a decimal), IRD% is the IRD abundance in the coarse-sand fraction (as a volume ratio), DBD is the dry bulk density of the whole sediment sample (in grams per cm^3) determined from discrete shipboard measurements and LSR is the interval average linear sedimentation rates (in cm kyr^{-1}).

Closed-form Fourier analysis was used to describe the shape of quartz grains in the IRD fraction imaged on a Quanta FEI 200 Scanning Electron Microscope (in the high vacuum mode at 20 kV) following methods that have been used to describe sedimentary particles for more than 40 years (Ehrlich and Weinberg, 1970; Ehrlich *et al*., 1980; Dowdeswell, 1982; Livsey *et al.,* 2013). Two-dimensional SEM images (from 200 to 500 X magnification) were input into ImageJ to produce a line trace of the boundary for each grain. The output was inspected to verify that the trace was representative of the grain. 120 xy coordinate points were output from the boundary to represent the grain and these were input into the software program PAST (Hammer *et al.,* 2001). Harmonic amplitudes 1-20 were calculated, lower orders (1-10) represent grain shape, a function of provenance and higher order harmonics (11-20) represent grain roundness (Dowdeswell, 1986; Haines and Mazzullo, 1988; Livsey *et al*., 2013). An average dimensionless roughness coefficient (Rca-b) was calculated for each sample using the

harmonics 16-20 for each grain in the population. Higher Rc16-20 values indicate increasing roughness and lower coefficients indicate smoother grains (Dowdeswell, 1982; Livsey *et al.*, 2013). The roughness coefficient is calculated as in Eq. (7):

$$Rc_{a-b} = \sqrt{0.5} \sum Rn^2 \tag{7}$$

Where Rn is the nth harmonic coefficient and a-b is the harmonic range used, in our case 16-20 (Ehrlich and Weinberg, 1970). This value represents the average roundness for the grains in each sample, numbering at least 25.

3.4 Pollen Analysis

Palynological treatments were performed on 13 samples according to the procedure routinely used at GEOTOP (de Vernal *et al.*, 1996). Before sieving and chemical treatments, one *Lycopodium clavatum* spore tablet was added in each sample to estimate palynomorph concentrations (Matthews, 1969; Mertens *et al.*, 2009). Wet sample volumes were measured by water displacement and weighed after being dried. The fraction between 10 and 120 μm was treated chemically to dissolve carbonate and silicate particles with repeated cold HCl (10 %) and HF (48 %). A small drop of the final residue was mounted on a microscope slide with glycerine jelly. Counting and identification of pollen grains and spores were carried out with a LEICA DM 5000B microscope.

4 Results and Discussion

4.1 Early and mid-Pliocene (4 to 3 Ma): early Cordilleran Ice Sheet and first glaciation attempts

Early to late-Pliocene (4 to 2.76 Ma) SSTs at Site U1417 are highly variable (max and min SST difference of 10 °C) with an average value of 8.2 °C (Fig. 2; Table 1). We compare our palaeo-SST with the modern SST (here "modern" refers to the averaged decadal statistical mean SST of 6.5 °C (standard deviation of 3.4 °C) during the 1955 to 2012 time period, NOAA WOD13; Boyer *et al.*, 2013) at the location of Site U1417 to observe changes in the behaviour of the Alaskan Current. Early to late-Pliocene average SSTs at Site U1417 were approximately 1.7 °C warmer than modern. The Pliocene and Pleistocene SSTs at the GOA have a similar SST range to modern (e.g. NOAA WOD13; Boyer *et al.,* 2013; Fig. 2). The MPWP (3.2 to 3.0 Ma) contains the highest SST peak of the Pliocene, SST=12.4 °C, 5.9 °C warmer than modern SST in the GOA. The average MPWP SST of 8.9 °C is around 2.4 °C warmer than modern. Similar to the MPWP, the MG1-Gi1 warm period (3.6 to 3.4 Ma) contains the second highest peak in SST during the Pliocene, SST=11.7 °C, 5.2 °C warmer SST than modern GOA. Other SST peaks during the MG1-Gi1 are 2-3 °C warmer than modern. The average SST during the MG1-Gi1 period is 9.5 °C, around 3 °C warmer than modern. $C_{37:4}$ concentrations during the Pliocene remain below the threshold of subpolar/subarctic water masses identified in the Nordic Seas (Bendle and Rosell-Melé, 2004) and are consistent with a warm surface ocean and/or minimal meltwater inputs to the GOA. The wide range of "warmer than modern" SSTs occurring during the MPWP together with higher than modern atmospheric CO_2 levels and similar continental configuration, further supports the proposal to use this time period as an analogue for future climate predictions (Hansen, 2006). The MG1-Gi1period

represents the opportunity for studies to focus on a prolonged period of sustained warm SST but with similar SST peaks than the MPWP.

During the early to mid-Pliocene, IRD is absent and sedimentation rates are the lowest of the 4-1.7 Ma record. Small glaciers in Alaska since or before 4 Ma have been indicated from neodymium and lead isotope records from the Bering Sea (Horikawa *et al.*, 2015). However, our data show that during the early and mid-Pliocene, the Cordilleran Ice Sheet was not yet extensive enough to erode or transport large volumes of sediment and runoff to the GOA. In contrast, IRD at ODP Site 887 (located 200 km southwest of U1417) suggests glacial influence in the GOA since 5.5 Ma (Reece *et al.*, 2011). Early Pliocene and even Miocene evidence of tidewater glaciation ($\delta^{18}O$, IRD) has been found at other locations in the North Atlantic (Mudelsee and Raymo, 2005; Bachem *et al.*, 2016). Reece *et al.* (2011) attributed the initiation of glaciation in the GOA to the uplift of the Yakutat formation. However, IRD mass accumulation rates at ODP 887 prior to 2.6 Ma are very small, being close to 0 and < $0.2 \text{ g cm}^{-2} \text{ Ky}^{-1}$ (Krissek, 1995). The low sedimentation rate, high TAR, low %$C_{37:4}$ and absence of IRD during this period at Site U1417 suggest that although the GOA experienced intervals of relatively cool SSTs (Fig. 2a), limited mountain glaciation but not full-scale continental glaciation resulting in tidewater glaciers marked the early and mid-Pliocene presented here.

There are two intervals of significant cooling recorded during the Pliocene at Site U1417: the MIS M2 (3.3 Ma) and KM2 (3.2 Ma) (Fig. 2a). Neither of these cold intervals record IRD delivery to Site U1417. Both intervals are punctuated by core breaks, suggesting a change in the sediment lithology which made core recovery difficult (Fig. S1). The M2 has been proposed as a significant Pliocene glaciation, though smaller than early Pleistocene glaciations, possibly due to the prevalent high atmospheric CO_2 levels (De Schepper *et al.*, 2013) (Fig. 3a). However, if this event, and the climatic conditions we record in the GOA, triggered the appearance of glaciation in Alaska at all (De Schepper *et al.*, 2013), our data suggests the glaciation was not intense enough to support an ice sheet with a tidewater margin that delivered icebergs to Site U1417. Our record provides evidence for relatively cold SST conditions during M2, as cold as conditions during major glacial cycles of the Pleistocene, but with no evidence for the development of a major Cordilleran Ice Sheet.

Between 4 and 3 Ma ago, we observe maximum TAR values (up to 16; Fig. 2), pointing to a higher export of terrigenous (i.e. land-plant leaf waxes) relative to aquatic organic matter to the GOA. We assume that the warm and wet climate of the early Pliocene during high atmospheric CO_2 levels potentially sustained a highly vegetated landscape in Alaska and west Canada which delivered high amounts of plant wax lipids and pollen grains into the GOA. The absence of IRD and higher pollen counts may refer to an airborne transport of the leaf wax lipids rather than an export via icebergs. The colder SST during the Pliocene could have promoted a deeper AL and dust driven transport of terrigenous organic matter may have developed. Strong winds could have transported plant waxes to Site U1417 during the Pliocene, as is also observed in the North Atlantic during the NHG (Naafs *et al.*, 2012). Müller *et al.* (2018) also proposed an export of long-chain *n*-alkanes to the GOA via dust storms. We suggest that, in addition to wind transport, also coastal river discharge of terrigenous organic matter may have contributed to higher TAR values recorded at Site U1417.
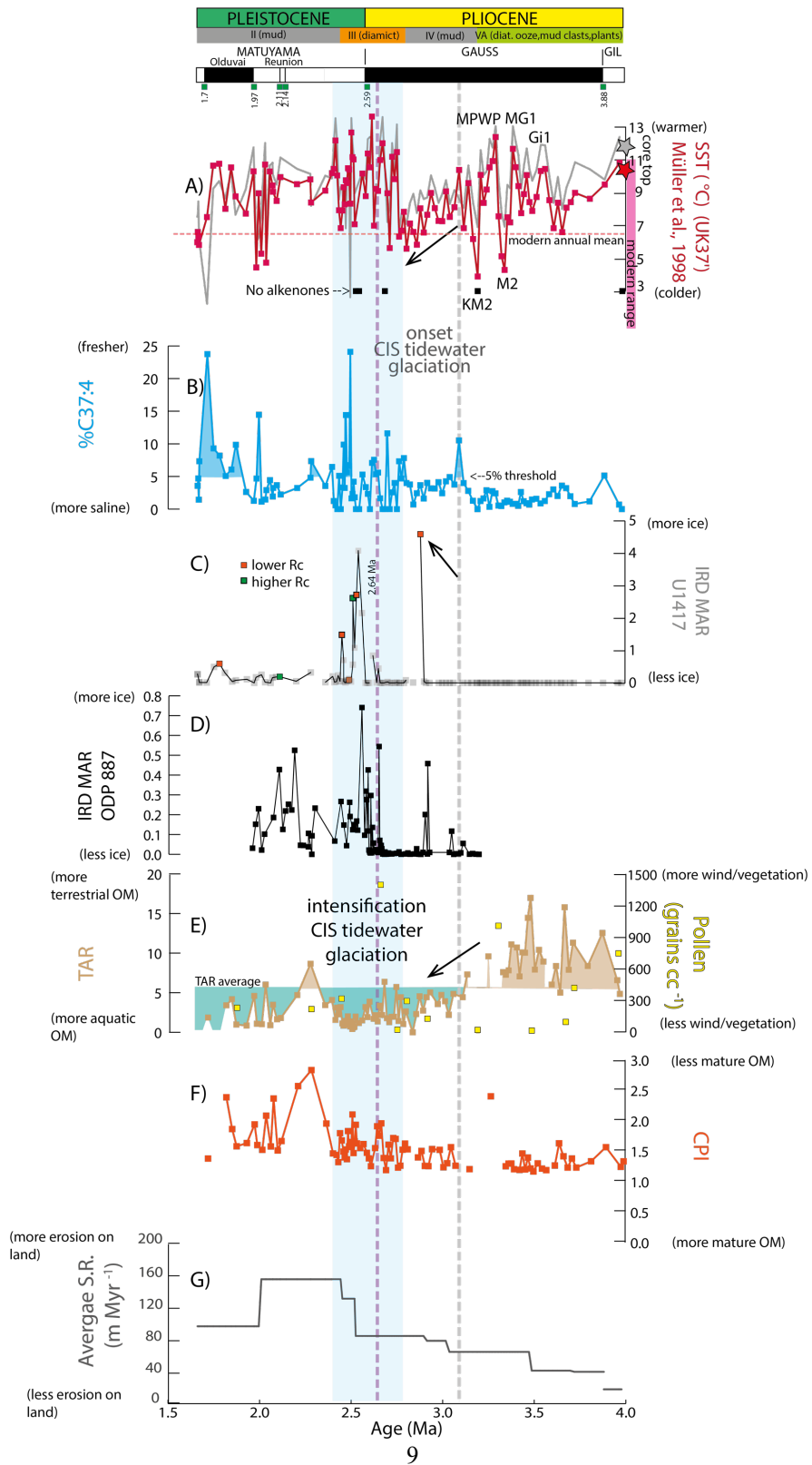
Figure 2: Site U1417 across the Pliocene-Pleistocene transition. a) red line: SST from U^K_{37}' index according to Müller *et al.* (1998) calibration; grey line: SST from U^K_{37} index according to Prahl *et al.* (1988) calibration. Black squares are samples where alkenones were not detected. Dashed red line: Modern averaged decades (1955-2012) annual statistical mean SST=6.4 °C at 0 m water depth (NOAA WOD13, Boyer *et al.,* 2013) at Site U1417, similar to the modern annual average SST=7 °C at GAK1 station during the 1970-2018 time
5   intervals for the 0-100 m water column depth (Weingartner *et al.* 2016) in the Gulf of Alaska; Red star on y-axis: value of our youngest sample analysed at Site U1417 (U1417D 1H-1W 44-48; 0.016 Ma; SST=10.6 °C with Müller *et al.* (1998) calibration; SST=11.8 °C with Prahl *et al.,* 1988 calibration); Pink rectangle on y axis: modern averaged decades (1955-2012) statistical mean SST during winter and summer at Site U1417 and 0 m water depth (NOAA WOD13, Boyer *et al.,* 2013) SST=0-11,3 °C; b) abundance of the cold and freshwater alkenone $C_{37:4}$ (%). Horizontal line shows the threshold of Bendle *et al.* (2005) above which subarctic/subpolar water masses were determined
10   for the Nordic Seas; c) IRD MAR (g cm^{-2} ka^{-1}). Orange and green squares reflect lower and higher average roughness coefficient (Rc) of the IRD quartz grains, respectively; d) IRD MAR (g cm^{-2} ka^{-1}) at ODP 887 (Prueher and Rea, 2001); e) terrestrial/aquatic *n*-alkane index (TAR), horizontal line shows the average TAR value, yellow squares represent pollen grains concentrations in grains cc^{-1} and f) CPI and g) average sedimentation rates (see Fig. S3b) in m Myr^{-1} at Site U1417. Upper panel: Pliocene-Pleistocene boundary, magnetostratigraphy events and interpretations (see Fig. S2 and S3) and Lithostratigraphic units of Site U1417 with simplified lithology (orange colouring represents ice
15   rafted diamict interbedded with mud, brown colouring represents marine mud and green colouring represents diatom ooze interbedded with debris flow deposits containing mud clasts and plant fragments) (Jaeger *et al.*, 2014). Grey vertical line represents the onset of the Cordilleran Ice Sheet (CIS) glaciation (or oNHG) climate transition at 3 Ma, blue shading represents the 2.5-2.0 Ma climate transition with the intensification of the Cordilleran Ice Sheet (CIS) tidewater glaciation (or iNHG) as in Table 1 Purple vertical line represents the onset of the Cordilleran Ice Sheet at the Lower Klondike Valley, Yukon interior (Hidy *et al.*, 2013; Fig. 1). Missing data points are either a result of
20   samples analysed for SSTs at the early stages of the project which were not subsequently analysed for n-alkane distributions, and the result of samples where chromatograms reflected poorly resolved *n*-alkane peaks.

We further note that rivers and ocean currents could have transported bedrock material from the Yakutat Terrain (Childress, 2016) to Site U1417, 700 km offshore from the Alaskan coast. This would imprint the sediments delivered to the ocean with an ancient signal of terrigenous organic matter, rather than reflecting erosion of contemporary 'fresh' organic matter from
25   vegetation and soils. The CPI is often used to estimate the maturity of the organic matter and determine its source. Previous studies suggest that elevated TAR values and CPI values close to 1 reflect coal particles found in sediments in the GOA (Rea *et al.*, 1995; Gulick *et al.*, 2015). However, the coal-bearing Kulthieth rocks (McCalpin *et al.*, 2011), have a TAR signature of a maximum value of 2 (Childress, 2016). Since Site U1417 TAR (up to 16) and CPI values (> 1) do not overlap with TAR (up to 2) and CPI (< 1) values found onshore (Childress, 2016), the TAR and CPI values at Site U1417 thus suggest a mix of
30   sources of organic matter during this time dominated by contemporaneous vegetation, although we cannot exclude the possibility of some coal erosion.

4.2 The late Pliocene onset of the Cordilleran Ice Sheet glaciation (3 to 2.8 Ma)

The interval from 3 to 2.8 Ma is characterised by a shift of climate conditions from those observed during the early and mid-Pliocene (Fig. 2) to more glacial conditions. At 3 Ma, average SSTs at Site U1417 remain relatively warm (around 8 °C), yet,
35   there is the first cooling evidence at Site U1417 deduced from $C_{37:4}$ crossing the threshold of 5 % (Bendle *et al.*; 2005). %$C_{37:4}$ increases can be related to colder sea surface conditions, but due to Site U1417's location and climatic context, we suggest that increases in %$C_{37:4}$ relate to meltwater discharge from the expanding ice-sheet. From 3.1 to 2.8 Ma, SST decreases gradually from 8 to 5.5 °C (Fig. 2a) recording again colder SSTs than the modern GOA. We attribute this 0.3 Ma progressive cooling to the oNHG in response to the overall decrease in the atmospheric CO_2 (Seki *et al.,* 2010; Martínez-Botí *et al.*, 2015).
40   From 3 Ma, TAR values decrease to below the average of the entire TAR record, indicating that transport of leaf-wax lipids to Site U1417 increased in comparison with the Pliocene, which may be related to an increase in erosion on land due to the

advancing ice-sheet. The coincident increase in average sedimentation rates (from 65 to 79 m Myr^{-1}) indicates a more efficient erosive agent onshore than before 3 Ma and/or a change in the source of terrestrial matter. However, CPI values at Site U1417 (Fig. 2e) remain similar to early and mid-Pliocene values, which suggests a similar source of the terrigenous organic matter. The most reasonable explanation is that the land was becoming increasingly ice covered, so that the erosion of vegetation and

5 terrigenous organic matter eroded and transported to the ocean increased.

The peak in %$C_{37:4}$ at 3 Ma is followed by lower %$C_{37:4}$ values (close to 5 %) and the first significant pulse of IRD identified by a single sample with the highest IRD MAR. This IRD MAR peak (4.5 g cm^{-2} ka^{-1}) and an increase in sedimentation rates (from 79 to 85 m Myr^{-1}) at 2.9 Ma constitute the first evidence that tidewater glaciers were present in southwest Alaska delivering icebergs to Site U1417. IRD quartz grains do not appear crushed or abraded by glacial activity indicating small

10 tidewater valley glaciers producing icebergs which could contain grains that were introduced by rockfall or fluvial sediment. The abrupt peak in IRD delivery to U1417 at 2.9 Ma could be due to ice growth on land and cold enough SSTs to permit distal iceberg-drift and release of debris to Site U1417. The increase in sedimentation rate has been suggested to mark the maximum Cordilleran Ice Sheet extension during the Pliocene (Gulick *et al*., 2015). Following this first peak, IRD MAR decreases to values between 0 and 1 g cm^{-2} ka^{-1} until 2.6 Ma. This abrupt decrease in IRD indicated lower iceberg delivery to Site U1417.

15 A synchronous increase of $C_{37:4}$ above 5 % suggests the melting of tidewater glaciers was responsible for the decrease in iceberg delivery despite the cold SST. Atmospheric CO_2 concentration peaks during this time (Fig. 3a) may have contributed to a reduced ice sheet due to radiative forcing.

4.3 The intensification of the Cordilleran Ice Sheet glaciation (2.7-2.4 Ma) and its evolution during the early Pleistocene (2.4-1.7 Ma)

20 At Site U1417, the iNHG during the Plio-Pleistocene transition (PPT) is characterised by a rise in SST, followed by highly variable values (between 5.6 to 13.6 °C) with an average of 9.7 °C, 3.2 °C warmer than modern. The iNHG is defined here as the period containing sustained signs of glaciation (i.e. Maslin *et al*.,1996; Bartoli *et al*., 2005), which at Site U1417 are confirmed by glacial meltwater and IRD delivery. The relatively high %$C_{37:4}$ (up to 24 %) in the early Pleistocene correlates well with the period of high IRD delivery (up to 4 g cm^{-2} Ka^{-1}) between 2.7 to 2.4 Ma (Fig. 2b and c). This suggests this period

25 marks an expansion/intensification of the Cordilleran glaciation following a gradual SST cooling during the oNHG. The timing of the increase in IRD at Site U1417 coincides with the increase in IRD at Site 887 (St John and Krissek, 1999) and the maximum extent of the CIS as recorded onshore in the eastern Cordillera by the extensive Klondike gravels at 2.64 Ma (+0.20/-0.18 Ma) (Hidy *et al.,* 2013). The lithology at Site U1417 includes diamict layers that alternate with bioturbated mud from 2.7 Ma, indicating that the Cordilleran Ice Sheet remained very variable after the oNHG and maintained glacial tidewater margins

30 discharging icebergs into the sea. Yet the intensification of the Alaskan tidewater glaciation occurred with a GOA that was overall either warmer than, or at least as warm as the mid to late Pliocene (considering Müller *et al*. 1998 SST calibration error).

The overall increase in %$C_{37:4}$ in the GOA during the early Pleistocene coincides with an SST warming (ca. 1 °C relative to the Pliocene; Fig. 2a and b), suggesting a stronger link between $C_{37:4}$ and meltwater fluxes rather than an expansion of subarctic water masses. Additionally, maxima and minima in %$C_{37:4}$ during the iNHG are unrelated to elevated or lowered SSTs, respectively. There is no information available about the origin of $C_{37:4}$ in the North Pacific to explain the high %$C_{37:4}$ values

5   recorded at Site U1417, nor their association with intermediate SSTs rather than minima/maxima. It has been suggested that stratification of the water column due to glacier discharge in the North Pacific could result in warmer sea surface in comparison to deeper water masses due to an increase in surface absorption of solar radiation (Meheust *et al.*, 2013). Haug *et al.* (2005) proposed this could lead to an increase in ocean evaporation and orogenic precipitation, ultimately encouraging North American ice sheet growth.

10   Over the iNHG, low TAR values (< 1) and small variations in IRD MAR (the order of 0.1 to 2.8 g cm^{-2} Ka^{-1}) coincide with intermediate SSTs (7 to 11 °C) and %$C_{37:4}$ between (2-24 %). This could point to an increase in marine productivity export related to an enhanced nutrient delivery to Site U1417 via glacial runoff. The CPI values discard mature sources of organic matter to the GOA at this time interval suggesting a contemporary aquatic organic matter contribution. IRD peaks are typically present during SST minima suggesting the importance of SSTs in the delivery of icebergs to distal sites such as Site U1417.

15   The average Rc of IRD is low (Fig. 2c) even during IRD MAR peaks, indicating minimal glacial crushing during the iNHG. In comparison, samples from 1.6 - 1.5 Ma show a higher Rc and appear to have greater evidence of glacial crushing, suggesting development of a larger ice sheet or scouring and evacuation of sediment from the non-glacial, weathered landscape. This could indicate that the first IRD in icebergs delivered to the GOA during the late Pliocene and early Pleistocene originated from smaller marine terminating valley glaciers which removed sediment and weathered rock from the landscape rather than

20   eroding bedrock and allowed IRD generation.

The comprehensive data set obtained from Site U1417 sediments (Fig. 2) supports a climate role in the ice-sheet expansion during the early Pleistocene and the iNHG, with an increase in precipitation from a warmer and/or stratified ocean, and cooler periods associated with IRD delivery. An additional explanation for the changing TAR during the early Pleistocene is that tectonic uplift of the Chugach/St Elias area from 2.7 Ma (Enkelmann *et al.*, 2015) led to orogenic precipitation and a change

25   in erosional pathways (Enkelmann *et al.*, 2015). The glaciation could have altered the main source of terrestrial input to the Surveyor Channel, to higher metamorphic and plutonic sources with lower or null TAR values (Childress, 2016). An increase in CPI variability to concentrations up to 2 and 3 during the early Pleistocene (starting from 2.7 Ma) supports the change of source of organic matter away from the more mature coal bedrock into more immature terrestrial organic matter (plant waxes). However, this comes at a time of increasing IRD, which adds a new source of terrigenous sediment to Site 1417. The shift in

30   CPI values at 2.7 Ma agrees with the shift towards the erosion of sediments sourced from metamorphic and plutonic sources, described in Enkelmann et al. (2015) delivered to Site U1417. Lower pollen counts suggest a less vegetated landscape, which could help explain the overall lower TAR during the early Pleistocene in comparison with the Pliocene.

4.4 The Pliocene and Pleistocene climate across the North Pacific Ocean.

The overall cooling trend during the Neogene, briefly interrupted by the MPWP and intense cooling events such as the M2, is believed to be a dominant pattern in the global climate. This notion is largely based on the global increase in ice volume (e.g. LR04 Benthic $\delta^{18}O$ Stack (Lisiecki and Raymo, 2005) and from studies in the North Atlantic SST (i.e. ODP Site 982, Lawrence *et al.*, 2009). In contrast, the contribution of the North Pacific into our understanding of the global climate evolution from the Pliocene to the Pleistocene is limited. Our study at Site U1417 adds valuable regional climate information during the evolution of the Cordilleran Ice Sheet. Unlike the LR04 stack, average Pliocene SST values (4.0 to 2.8 Ma) at Site U1417 are 1 °C colder than the average early Pleistocene values (2.7 to 1.7 Ma) (the Pliocene-Pleistocene SST difference of 1°C has an standard deviation of 0.5°C). In the wider North Pacific, a warming trend from the late Pliocene to early Pleistocene has also been observed at ODP Site 882 in the subarctic Pacific (Martínez-García *et al.*, 2010), at Site 1010 and potentially at Site 1021 (mid-latitude east Pacific) (Fig. 3). Beyond the North Pacific, warmer SST during the early Pleistocene compared to the Pliocene have also been recorded i.e. DSDP Site 593 in the Tasman Sea (McClymont *et al.*, 2016) and Site 1090 (Martínez-García *et al.*, 2010) in the South Atlantic. In contrast, long-term cooling trends mark the early Pleistocene for the mid-latitude west Pacific (Site 1208) and tropical east Pacific (Site 846), more consistent with the development of a cooler and/or more glaciated climate (Fig. 3).

The North Pacific warming occurs despite an atmospheric CO_2 drop from 280-450 ppmv to 250-300 ppmv (similar to pre-industrial levels) from 3.2 to 2.8 Ma (Pagani *et al.*, 2010; Seki *et al.*, 2010) and an associated reduction in global radiative forcing (Foster *et al.*, 2017). The early Pleistocene warming signal in the GOA (and the north Pacific more generally) thus implies an important role for local or regional processes. We have discussed above the potential role played by ocean stratification in the North Pacific, and a possible link to the evolving Cordilleran Ice Sheet in the GOA through evaporation/precipitation feedbacks. The synchrony of these changes with observed tectonic uplift (e.g. Enkelmann *et al.* 2015) makes it difficult to disentangle the potential climatic and tectonic mechanisms behind ice sheet expansion.

To understand the evolution of the ocean currents governing the North Pacific at the present core sites (Fig. 1) and to find possible explanations of the observed SST distributions during the Pliocene and Pleistocene climate evolution, the modern climate system is used here as an analogue. Modern monthly mean SSTs at ODP 882 SSTs are colder than Sites U1417 and 1021 all year around. During the late Pliocene and early Pleistocene, ODP 882 SSTs are 3-4 °C warmer than in the east (Fig. 3f and g). Modern seasonal climate analogues cannot be used to explain to Pliocene and Pleistocene subarctic SST distribution. However, on longer timescales, the strength of the AL is currently linked to the wider Pacific Ocean circulation by the Pacific Decadal Oscillation (PDO) over periods of 20-30 years (Furtado *et al.*, 2011). The Pliocene-Pleistocene North Pacific SST gradients show similarities with the negative phase of the PDO (-PDO), which is characterized by positive SST anomalies in the central North Pacific surrounded by negative SST anomalies along the North American coast and in the east equatorial

Pacific. The -PDO associated route of winds might have increased the precipitation in the Gulf of Alaska and represent a key factor for the fast building of ice in the Alaskan mountains.
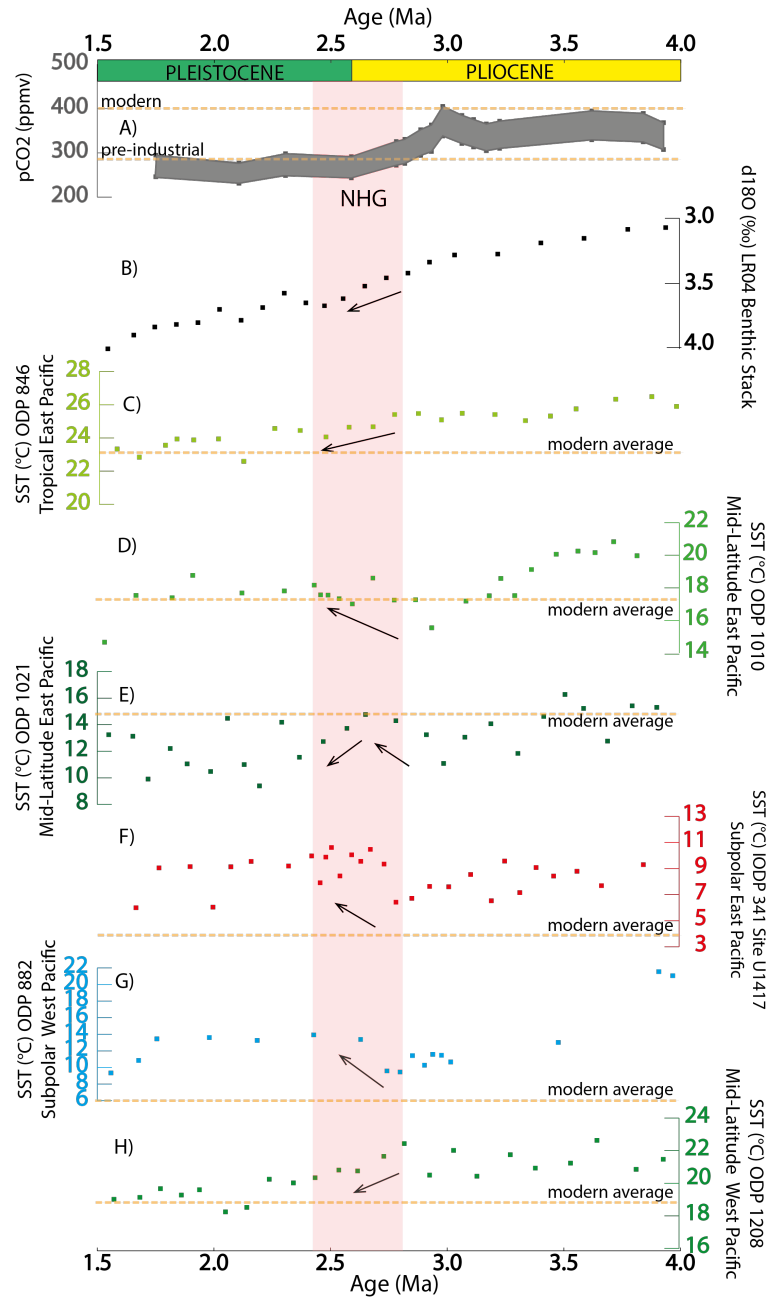
Figure 3: **Pliocene-Pleistocene SST across the North Pacific.** a) Alkenone pCO_2 upper and lower end (ppmv) estimates at Site ODP 999A (Seki *et al.,* 2010); b) $\delta^{18}O$ (‰) LR04 Benthic Stack (Lisiecki and Raymo, 2005); Alkenone SST (°C) from c) ODP Site 846 (Herbert *et al.,* 2017), d) Site 1010 (Herbert *et al.,* 2018), e) Site 1021 (Herbert *et al.,* 2018), f) IODP 341 Exp. Site U1417 (Sánchez-Montes *et al.,* 2019), g) ODP Site 882 (Martínez-García *et al.,* 2010) and h) ODP Site 1208 (Herbert *et al.,* 2018). Orange horizontal lines indicate reference levels

of pre-industrial times and/or modern values for each of the records or sites (SSTs from NOAA WOD13, Boyer *et al.*, 2013). Arrows indicate position of M2 and KM2 periods and cooling or warming trends across the Pacific Ocean. The KM2 event is located within the MPWP. The MG1-Gi warming precedes the M2 event. b) to h) climate data are 100 kyr smoothed records, and the x axis have been determined through the calculation of the mean for each interval.

5 Conclusions

The sea surface temperature (SST) evolution from the Pliocene to the early Pleistocene in the subarctic Northeast and east-mid latitude North Pacific is very different from the North Atlantic, with a colder Pliocene than early Pleistocene. The early Pliocene appears to be characterised by a heavily vegetated landscape where there is no obvious noticeable glaciation in the

10 St. Elias mountains. A series of cooling events during the Pliocene (including the M2 event) could have initiated glaciation in Alaska but it was limited to mountain glaciers probably due to high atmospheric CO_2 concentrations and the lower topography in coastal Alaska. The first evidence of glaciation starts at 3 Ma with an increase in glacial meltwater followed by a progressive 2.5 °C SST cooling from 3.1 to 2.8 Ma and the first IRD peak at 2.9 Ma since the late Pliocene. Glacial meltwater, IRD and sedimentation rates increase, identified as the intensification of the Cordilleran glaciation (2.7-2.4 Ma). This occurs with warm

15 SSTs suggesting an efficient warm ocean-land precipitation-Cordilleran Ice Sheet growth interactions.

A permanent warm surface ocean in the west mid-latitude Pacific during the late Pliocene and early Pleistocene compared to modern was potentially a key mechanism for increasing moisture supply to the Gulf of Alaska (GOA) and triggering the growth of the Cordilleran Ice Sheet. A similar to modern negative PDO-like climate could have set a more efficient route for moisture transport from the west subarctic Pacific to the GOA since the MPWP and could have been a key mechanism for glacial

20 growth. Unlike during the Pliocene, the early Pleistocene drop in atmospheric CO_2 concentrations could have been decisive in developing a continuous glaciation of the Cordilleran Ice Sheet during the variable climate of the intensification of the Cordilleran tidewater glaciation. However, the synchronous tectonic uplift of the St Elias mountains could also have been a contributing factor for the Cordilleran Ice Sheet expansion, increasing the potential for precipitation as snow over the ice sheet source regions, despite warm SST in the GOA.

Data availability

The data presented in this manuscript has been submitted to Pangaea.de and it is under review. After the publication of this manuscript, the data would be accessible through this link https://doi.org/10.1594/PANGAEA.899064 and could be cited as Sánchez-Montes *et al*. (2019). The SST data in this publication will also be published in the PlioVAR database.

Author contribution

New data sets presented in this manuscript derive from the PhD project of MLSM supervised by ELM and JML. JM was closely engaged from early stages of this project including aspects of method development. EAC generated the IRD data, and CZ generated pollen data. All authors have contributed to data interpretations. MLSM prepared the manuscript with contributions from all co-authors.

Acknowledgements

We would like to acknowledge the International Ocean Discovery Program U.S. Implementing Organization (IODP-USIO) and the captain and crew of the D/V *Joides Resolution*. This work was supported by funding from Van Mildert College and the Durham Doctorate Scholarship (MLSM), the Philip Leverhulme Prize (ELM), and a NERC-IODP grant (NE/L002426/1) to ELM. JM received funding through the German Research Foundation (MU3670/1-2), an ECORD grant and the Helmholtz Association (VH-NG-1101). EAC received funding from U.S. National Science Foundation award OCE-1434945 and a post-expedition award from the U.S. Science Support Program of the IODP. We thank valuable comments from Professor Joseph S. Stoner on our new age model proposed here. We thank Martin West, Amanda Hayton and Kathryn Melvin for assistance with the GCMS analyses, and Mathew Sandefur and Hugh Harper for assistance with the IRD analyses. This work is a contribution to the PlioVAR working group synthesis of Pliocene marine data (http://pastglobalchanges.org/). We thank Alberto Reyes (CP editor) and CP reviewers Anders Carlson and a second anonymous reviewer for valuable discussions and comments that helped in shaping this manuscript.

References

Andreev, A. A., Trasov, P. E., Weenrich, V., Raschke, E., Herzschuh, N. R., Bringham-Grette, J. and Melles, M., Late Pliocene and Early Pleistocene vegetation history of northeastern Russian Arctic inferred from the Lake El'gygytgyn pollen record, Clim. Past, 10, 1017-1039, 2014.

Bachem, P.E., Risebrobakken, B. & McClymont, E.L. Sea surface temperature variability in the Norwegian Sea during the late Pliocene linked to subpolar gyre strength and radiative forcing. Earth and Planetary Science Letters, 446:113- 122, 2016.

Bartoli, Gretta; Sarnthein, Michael; Weinelt, Mara; Erlenkeuser, Helmut; Garbe- Schönberg, Carl-Dieter; Lea, David W, Final closure of Panama and the onset of northern hemisphere glaciation. Earth and Planetary Science Letters, 237, 33-44, doi:10.1016/j.epsl.2005.06.020, 2005.

Bendle, J. A.; Rosell-Melé, A., Ziveri, P., Variability of unusual distributions of alkenones in the surface waters of the Nordic seas, Paleoceanography, 20(2), PA2001, doi:10.1029/2004PA001025, 2005.

Bendle, J. A. and Rosell-Melé, A., Distributions of UK37 and UK37' in the surface waters and sediments of the Nordic Seas: implications for paleoceanography. Geochemistry, Geophysics, Geosystems 5, Q11013-Q11013, doi:10.1029/2004GC000741, 2004.

Boyer, T.P., Antonov, J. I., Baranova, O. K, C. Coleman, C., García, H. E., Grodsky, A., Johnson, D. R., Locarnini, R. A. Mishonov, A. V., O'Brien, T.D., Paver, C.R., Reagan, J.R., Seidov, D., Smolyar, I. V. and Zweng, M. M., World Ocean Database, NOAA Atlas NESDIS 72, S. Levitus, Ed., A. Mishonov, Technical Ed.; Silver Spring, MD, 209 pp., http://doi.org/10.7289/V5NZ85M , 2013.

Bray, R. R. and Evans, E. D., Distribution of n-paraffins as a clue to recognition of source beds, Geochimica et Cosmochimica Acta, 22, 2-15, 1961.

Bringham-Grette, J., Melles, M., Minyuk, P., Andreev, A., Tarasov, P., Deconto, R., Koenig, S., Nowaczyk, N., Wennrich, V, Rosén, P., Haltia, E., Cook, t., Gebhardt, C., Meyer-Jacob, C., Snyder, J., Herzschuh, U., Pliocene warmth, polar amplification, and stepped pleistocene cooling recorded in NE Arctic Russia, Science, 340(6139), 1421-1427, https://doi.org/10.1126/science.1233137, 2013.

Childress, L. B., The Active Margin Carbon Cycle: Influences of Climate and Tectonics in Variable Spatial and Temporal Records, PhD thesis Northwestern University, Evanson, Illinois, 2016.

Cranwell, P. A, Chain-length distribution of n-alkanes from lake sediments in relation to post-glacial environmental change, Freshwater Biol. 3:259-265, 1973.

De Shepper, S., Groeneveld, J., Naafs, B. D., Van Renterghem, C., Hennissen, J., Head, M. J., Louwye, S. and Fabian, K., Northern Hemisphere Glaciation during the Globally Warm Ealy Late Pliocene, PLOS ONE, Vol. 8, Issue 12, 1-15, 2013.

de Vernal, A., Henry, M., Bilodeau, G., Micropaleontological preparation techniques and analyses. Les Cahiers du Geotop 3, 16–27, 1996.

Dolan, A. M., Haywood, A. M., Hill, D. J., Dowsett, H. J., Hunter, S. J., Lunt, D. J. and Pickering, S. J., Palaeogeography, Palaeoclimatology, Palaeoecology 309, 98-110, 2011.

Dolan, A. M., Haywood, A. M., Hunter, S. J., Tindall, J. C., Dowsett, H. J., Hill, D. J. and Pickering, S. J., Modelling the enigmatic Late Pliocene Glacial Event, Marine Isotope Stage M2, Global and Planetary Change 128, 47-60, 2015.

Dowdeswell, J.A., Scanning electron micrographs of quartz sand grains from cold environments examined using fourier shape analysis, Journal of Sedimentary Petrology 52, 1315-1323, 1982.

Dowdeswell, J.A., The distribution and character of sediments in a tidewater glacier, southern Baffin Island, N.W.T., Canada, Arctic and Alpine Research 18, 45-56, 1986.

Ehrlich, R. and Weinberg, B., An exact method for characterization of grain shape, Journal of Sedimentary Petrology 40, 205-212, 1970.

Ehrlich, R., Brown, P.J., Yarus, J.M. and Przygocki, R.S., The origin of shape frequency distributions and the relationship between size and shape, Journal of Sedimentary Petrology 50, 475-483, 1980.

5   Enkelmann, Peter O. Koons, Terry L. Pavlis, Bernard Hallet, Adam Barker, Julie Elliott, John I. Garver, Sean P. S. Gulick, Rachel M. Headley, Gary L. Pavlis, Kenneth D. Ridgway, Natalia Ruppert, Harm J. A. Van Avendonk. Cooperation among tectonic and surface processes in the St. Elias Range, Earth's highest coastal mountains. Geophysical Research Letters, 42 (14): 5838 DOI: 10.1002/2015GL064727, 2015.

Fedorov, A. V., Lawrence, K. T., Liu, Z., Dekens, P. S., Ravelo, A. C., and Brierley, C. M.: Patterns and mechanisms of early

10 Pliocene warmth, Nature, 496, 43–49, doi:10.1038/nature12003, 2013.

Foster, G. L. et al. Future climate forcing potentially without precedent in the last 420 million years. Nat. Commun. 8, 14845 doi: 10.1038/ncomms14845, 2017.

Furtado, J. C., Di Lorenzo, E., Schneider, N. and Bond, N.A., North Pacific Decadal Variability and Climate Change in the IPCC AR4 Models, American Meteorological Society, Vol. 24, 3049-3067, 2011.

15 Gulick, S. P. S., Jaeger, J. M., Mix, A. C., Asahi, H., Bahlburg, H., Belanger, C. L.,Berbel., G. B. .B, Childress, L., Cowan, E., Drab, L., Forwick, M., Fukumura, A, Ge, S., Gupta, S., Kiola, A., Konno, S., LeVay, L. J., Marz, C., Matsuzaki, K. M., McClymont, E. L., Moy, C., Müller, J., Nakamura, A., Ojima, T., Ribeiro, F. R., Ridgway, K. D., Romero, O. E., Slagle, A. L., Stoner, J. S., St-Onge, G., Suto, I., Walczak, M. D., Worthington, L. L., Bailey, I., Enkelmann, E., Reece, R. and Swartz, J.M., Mid-Pleistocene climate transition drives net mass loss from rapidly uplifting St. Elias Mountains, Alaska. Proceedings

20 of the National Academy of Sciences of the United States of America, 112(49), 15042–15047. http://doi.org/10.1073/pnas.1512549112, 2015.

Haines, J., and Mazzullo, J., The original shape of quartz silt grains: a test of the validity of the use of quartz grain shape analysis to determine the source of terrigneous silt in marine sedimentary deposits, Marine Geology 78, 227-240, 1988.

Hansen, J., Sato, M., Ruedy, R., Lo, K., Lea, D. & Medina-Elizalde, M., Global temperature change. Proc. Natl Acad. Sci.

25 USA 103, 14 288–14 293, doi:10.1073/pnas.0606291103, 2006.

Harada, N., Sato, M., Shiraishi, A. and Honda, M.C., *Characteristics of alkenone distributions in suspended and sinking particles in the northwestern North Pacific*, Geochim. Cosmochim. Acta, 70, pp. 2045–2062, 2006.

Haug, G. H., Ganopolski, A., Sigman, D. M., Rosell-Mele, A., Swann, G. E. A., Tiedemann, R., Jaccard, S. L., Bollmann, J., Maslin, M A., Leng, M. J. and Eglinton, G., North Pacific seasonality and the glaciation of North America 2.7 million

30 years ago, Nature, vol 433, 821-825, 2005.

Haug, G. H., Sigman, D. M., Tiedemann,R., Pedersen, T. F. and Sarnthein, M., Onset of Permanent stratification in the subarctic Pacific Ocean, Letters to Nature, Vol. 401, 779-782, 1999.

Haywood, A.M., Dolan, A.M., Pickering, S.J., Dowsett, H.J., McClymont, E.L., Prescott, C.L., Salzmann, U., Hill, D.J., Hunter, S.J., Lunt, D.J., Pope, J.O., Valdes, P.J., On the identification of a Pliocene time slice for data–model comparison. Philos. Trans. R. Soc., Math. Phys. Eng. Sci. 371, 20120515. http://dx.doi.org/10.1098/ rsta.2012.0515, 2013a.

Haywood, A. M. and Valdes, P. J., Modelling Pliocene warmth: contribution of atmosphere, oceans and cryosphere, Earth and Planetary Science Letters, 218, pp.363-377. doi: 10.1016/S0012-821X(03)00685-X , 2004.

Herbert, Timothy D; Lawrence, Kira T; Tzanova, Alexandrina; Peterson, Laura C; Caballero-Gill, Rocio P; Kelly, Christopher S (Table S2) SST estimates as a function of age, ODP Site 167-1010, PANGAEA, 2018, https://doi.org/10.1594/PANGAEA.885599, In supplement to: Herbert, TD et al., Late Miocene global cooling and the rise of modern ecosystems. Nature Geoscience, 9(11), 843-847, https://doi.org/10.1038/ngeo2813, 2016.

Herbert, Timothy D; Lawrence, Kira T; Tzanova, Alexandrina; Peterson, Laura C; Caballero-Gill, Rocio P; Kelly, Christopher S, (Table S2) SST estimates as a function of age, ODP Site 167-1021. PANGAEA, 2018, https://doi.org/10.1594/PANGAEA.885579, 2018. In supplement to: Herbert, TD et al. Late Miocene global cooling and the rise of modern ecosystems. Nature Geoscience, 9(11), 843-847, https://doi.org/10.1038/ngeo2813, 2016.

Herbert, Timothy D; Lawrence, Kira T; Tzanova, Alexandrina; Peterson, Laura C; Caballero-Gill, Rocio P; Kelly, Christopher S, (Table S2) SST estimates as a function of age, ODP Hole 198-1208A. PANGAEA, 2018, https://doi.org/10.1594/PANGAEA.885584, 2018. In supplement to: Herbert, TD et al., Late Miocene global cooling and the rise of modern ecosystems. Nature Geoscience, 9(11), 843-847, https://doi.org/10.1038/ngeo2813, 2016.

Herbert, Timothy D; Peterson, Laura C; Lawrence, Kira T; Liu, Zhonghui, Plio-Pleistocene tropical alkenone SST reconstructions for ODP Site 138-846. PANGAEA, 2017, https://doi.org/10.1594/PANGAEA.874750, In supplement to: Herbert, TD et al., Tropical Ocean Temperatures Over the Past 3.5 Million Years. Science, 328(5985), 1530-1534, https://doi.org/10.1126/science.1185435, 2010.

Hidy, A. J., Gosse, J. C., Froese, D. G., Bond, J. D., and Rood, D. H.: A latest Pliocene age for the earliest and most extensive Cordilleran Ice Sheet in northwestern Canada, Quaternary Res., 61, 77–84, doi:10.1016/j.quascirev.2012.11.009, 2013.

Hogan, C., *Oceans and Seas Gulf of Alask*a, The Encyclopedia of Earth, http://www.eoearth.org/view/article/153188 (date accessed 13/11/2015), 2013.

Horikawa, K., Martin, E. E., Basak, C., Onodera, J., Seki, O., Sakamoto, T., Ikehara, M., Sakai, S. and Kwamura, K., Pliocene cooling enhanced by flow of low-salinity Bering Sea water to the Arctic Ocean, Nature Communications, 6:7587, 2015.

Jaeger, J.M., Gulick, S.P.S., LeVay, L.J., Asahi, H., Bahlburg, H., Belanger, C.L., Berbel, G.B.B., Childress, L.B., Cowan, E.A., Drab, L., Forwick, M., Fukumura, A., Ge, S., Gupta, S.M., Kioka, A., Konno, S., Marz, C.E., Matsuzaki, K.M., McClymont, E.L., Mix, A.C., Moy, C.M., Müller, J., Nakamura, A., Ojima, T., Ridgway, K.D., Rodrigues Ribeiro, F., Romero, O.E., Slagle, A.L.,Stoner, J.S., St-Onge, G., Suto, I., Walczak, M.H., and Worthington, L.L., 2014. Site U1417. In Jaeger, J.M., Gulick, S.P.S., LeVay, L.J., and the Expedition 341 Scientists, Proc. IODP, 341: College Station, TX (Integrated Ocean Drilling Program). doi:10.2204/iodp.proc.341.103, 2014.

Jansen, E., J. Overpeck, K.R. Briffa, J.-C. Duplessy, F. Joos, V. Masson-Delmotte, D. Olago, B. Otto-Bliesner, W.R. Peltier, S. Rahmstorf, R. Ramesh, D. Raynaud, D. Rind O. Solomina, R. Villalba, and D. Zhang, Palaeoclimate. In Climate Change 2007: The Physical Science Basis. Contribution of Working Group I to the Fourth Assessment Report of the Intergovernmental Panel on Climate Change. S. Solomon, D. Qin, M. Manning, Z. Chen, M. Marquis, K.B. Averyt, M. Tignor, and H.L. Miller, Eds. Cambridge University Press, 433-497, 2007.

Kato, Y., Onodera, J., Suto, I., Teraishi, A. and Takahashi, K., *Pliocene and Pleistocene paleoceanography in the western subarctic Pacific based on diatom analyses of ODP Leg 145 Hole 884B and IODP Expedition 323 Holes U1341B and U1343E*, Deep-Sea Res. II, vol. 125-126, 29-37, 2016.

Knies, J. et al. The emergence of modern sea ice cover in the Arctic Ocean. Nat. Commun. 5:5608 doi: 10.1038/ncomms6608, 2014.

Kornilova, O. and Rosell-Mele, A., Application of microwave-assisted extraction to the analysis of biomarker climate proxies in marine sediments, Organic Geochemistry, 34, 1517–1523, 2003.

Krissek, L. A., Late Cenozoic Ice-Rafting Records From Leg 145 Sites In The North Pacific: Late Miocene Onset, Late Pliocene Intensification and Pliocene-Pleistocene Events, in Rea D. K. Basov, L. A., Scholl, D. W. and Allan, J.F., Proceedings of the Ocean Drilling Scientific Results, Vol 145, 1995.

Lawrence, K. T., Herbert, T. D., Brown, C. M., Raymo, M. E. and Haywood, A. M., High-amplitude variations in North Atlantic sea surface temperature during the early Pliocene warm period, Paleoceanography, 24, PA2218, https://doi.org/10.1029/2008PA001669, 2009.

Lawrence, K. T., Sosdian, S., Wite, H. E. and Rosenthal, Y., North Atlantic climate evolution trough the Plio-Pleistocene climate transitions, Earth and Planetary Science Letters 300, 329-342, 2010.

Lisiecki, Lorraine E; Raymo, Maureen E, Pliocene-Pleistocene stack of globally distributed benthic stable oxygen isotope records. PANGAEA, https://doi.org/10.1594/PANGAEA.704257,2005. Supplement to: Lisiecki, LE; Raymo, ME, A Pliocene-Pleistocene stack of 57 globally distributed benthic d18O records. Paleoceanography, 20, PA1003, https://doi.org/10.1029/2004PA001071, 2005.

Livsey, D.N., Simms, A.R., Clary, W.G., Wellner, J.S., Anderson, J.B., and Chandler, J.P., Fourier grain-shape analysis of Antarctic marine core: the relative influence of provenance and glacial activity on grain shape, Journal of Sedimentary Research 83, 80-90, 2013.

Locarnini, R. A., A. V. Mishonov, J. I. Antonov, T. P. Boyer, H. E. Garcia, O. K. Baranova, M. M. Zweng, C. R. Paver, J. R. Reagan, D. R. Johnson, M. Hamilton, and D. Seidov, 2013. *World Ocean Atlas 2013, Volume 1: Temperature.* S. Levitus, Ed., A. Mishonov Technical Ed.; NOAA Atlas NESDIS 73, 40 pp.

Martínez-Botí, M. A., Foster, G. L. Chalk, T. B., Rohling, E. J., Sexton, P. F., Lunt, D. J., Pancost, R. D., Badger, M. P. S., Schmidt. D. N., Plio-Pleistocene climate sensitivity evaluated using high-resolution CO_2 records. Nature, 518 (7537): 49 DOI: 10.1038/nature14145, 2015.

Martínez-García, A., Rosell-Mele, A., McClymont, E.L., Gersonde, R. & Haug, G. Subpolar Link to the Emergence of the Modern Equatorial Pacific Cold Tongue, Science, 328: 1550-1553, 2010.

Martínez-García, Alfredo; Rosell-Melé, Antoni; McClymont, Erin L; Gersonde, Rainer; Haug, Gerald H, (Table S3) Sea surface temperature and relative abundance of $C_{37:4}$ alkenone in ODP Site 145-882. PANGAEA, https://doi.org/10.1594/PANGAEA.771707, 2010. In supplement to: Martínez-García, A et al. (2010): Subpolar Link to the Emergence of the Modern Equatorial Pacific Cold Tongue. Science, 328(5985), 1550-1553, https://doi.org/10.1126/Science.1184480.

Martrat, B., Grimalt, J. O., Shackleton, N. J., de Abreu, L., Hutterli, M. A. and Stocker, T. F., *Four Climate Cycles of Recurring Deep and Surface Water Destabilizations on the Iberian Margin*, Science Volume 317, 5837, 502-507, 2007.

März, C., Schnetger, B., and Brumsack, H.-J2013, Nutrient leakage from the North Pacific to the Bering Sea (IODP Site U1341) following the onset of Northern Hemispheric Glaciation?, Paleoceanography, 28, 68–78, doi:10.1002/palo.20011, 2013.

Maslin, M.A., Haug, G.H., Sarnthein, M., Tiedemann, R., The progressive in- tensification of Northern Hemisphere glaciation as seen from the North Pacific, Geol. Rundsch 85, 452–465, 1996.

Matthews, J., The Assessment of a Method for the Determination of Absolute Pollen Frequencies. New Phytologist 68, 161–166, 1969, https://doi.org/10.1111/j.1469-8137.1969.tb06429.x.

Matthiessen, J., Knies, J., Vogt, C. and Stein, R., Pliocene palaeoceanography of the Arctic Ocean and subarctic seas, Phil. Trans. R. Soc. A (2009) 367, 21–48 doi:10.1098/rsta.2008.0203, 2008.

McCalpin, J. P., Bruhn, R. L., Pvlis, T. L., Gutierres, F., Guerrero, J. and Lucha, P., Antislope scarps, gravitational spreading, and tectonic faulting in the western Yakutat microplate, south coastal Alaska, Geosphere, 7 (5): 1143-1158, 2011.

McClymont, E.L., Elmore, A.C., Kender, S., Leng, M.J., Greaves, M. and Elderfield, H., Pliocene-Pleistocene evolution of sea surface and intermediate water temperatures from the southwest Pacific, Paleoceanography, 31, 895-913, 2016.

McClymont, E.L., Rosell-Melé, A., Haug, G. and Lloyd, J.M., *Expansion of subarctic water masses in the North Atlantic and Pacific oceans and implications for mid-Pleistocene ice sheet growth*, Paleoceanography, 23, PA4214, 2008.

Meheust, M., Fahl, K. and Stein, R., Variability in modern sea surface temperature, sea ice and terrigenous input in the sub-polar North Pacific and Bering Sea: Reconstruction from biomarker data, Organic Geochemistry 57, 54-64, 2013.

Mertens, K.N., Verhoeven, K., Verleye, T., Louwye, S., Amorim, A., Ribeiro, S., Deaf, A.S., Harding, I.C., De Schepper, S., González, C., Kodrans-Nsiah, M., De Vernal, A., Henry, M., Radi, T., Dybkjaer, K., Poulsen, N.E., Feist-Burkhardt, S., Chitolie, J., Heilmann-Clausen, C., Londeix, L., Turon, J.L., Marret, F., Matthiessen, J., McCarthy, F.M.G., Prasad, V., Pospelova, V., Kyffin Hughes, J.E., Riding, J.B., Rochon, A., Sangiorgi, F., Welters, N., Sinclair, N., Thun, C., Soliman, A., Van Nieuwenhove, N., Vink, A., Young, M., Determining the absolute abundance of dinoflagellate cysts in recent marine sediments: The Lycopodium marker-grain method put to the test. Review of Palaeobotany and Palynology 157, 238–252, 2009, https://doi.org/10.1016/j.revpalbo.2009.05.004.

Molnia, B.F., *Glaciers of North America -- Glaciers of Alaska*, in Williams, R.S., Jr., and Ferrigno, J.G., eds., Satellite image atlas of glaciers of the world: U.S. Geological Survey Professional Paper 1386-K, 525 p, 2008.

Mudelsee, M. and Raymo, M. E., Slow dynamics of the Northern Hemisphere glaciation, Paleoceanography, vol 20, PA4022, 2005.

Müller P. J., Kirst G., Ruhland G., von Storch I., and RosellMelé A., Calibration of the alkenone paleotemperature index UK37' based on core-tops from the eastern South Atlantic and the global ocean (608 N–608 S), Geochim. Cosmochim. Acta 62, 1757–1772, doi:10.1016/S0016-7037(98)00097-0, 1998.

Müller, J., Romero, O. Cowan, E. A., McClymont, E. L., Forwick, M., Asahi, H., Marz, C., Moy, C. M., Suto, I., Mix, A. and Stoner, J., Cordilleran ice-sheet growth fueled primary productivity in the Gulf of Alaska, northeast Pacific Ocean, Geology, v. 46; no. 4; p. 307–310, 2018.

Naafs, B. D. A., Hefter, J., Acton, G., Haug, G. H., Martínez-García, A., Pancost, R. and Stein, R., Strengthening of the North American dust sourcesduring the late Pliocene (2.7 Ma), Earth and Planetary Science Letters 317-318, 8-19, http://dx.doi.org/10.1016/j.epsl.2011.11.026, 2012.

Nie, J. et al. Pacific freshening drives Pliocene cooling and Asian monsoon intensification. Sci. Rep. 4, 5474; DOI:10.1038/srep05474, 2014.

Pagani, M., Liu, Z., La Riviere, J. and Ravelo, A. C., High Earth-system climate sensitivity determined from Pliocene carbon dioxide concentrations, Nature Geoscience, Vol 3., 27-30, 2010.

Pickart, RS, Macdonald, A. M., Moore, G. W. K., Renfrew, I. A., Walsh, J. E. and Kessler, W. S., 2009, *Seasonal evolution of Aleutian low pressure systems: implications for the North Pacific subpolar circulation*. J Phys Oceanogr 39, 1317– 1339, 2009.

Powell, R. D., and Molnia, B. F., Glacimarine sedimentary processes, facies and morphology of the south-southeast Alaska shelf and fjords, Mar. Geol., 85, 359–390, doi:10.1016/0025-3227(89)90160-6, 1989.

Prahl F. G., Muehlhausen L. A., and Zahnle D. L., Further evaluation of long-chain alkenones as indicators of paleoceanographic conditions, Geochim. Cosmochim. Acta 52, 2303–2310, 1988.

Prueher, Libby M; Rea, David K: (Table 1) Age, magnetic susceptibility, and mass accumulation rate of volcanic glass and IRD from ODP Site 145-887. PANGAEA, https://doi.org/10.1594/PANGAEA.706309, 2001.

Raymo, M. E., Grant, B., Horowitz, M. and Rau, G. H., Mid-Pliocene warmth: stronger greenhouse and stronger conveyor, Marine Micropalaeontology 27, 313-326, 1996.

Rea, D. K., Basov, I. A., Krissek, L. A. and the Leg 145 Scientific Party, *Scientific Results of drilling the North Pacific Transect*, in Rea, D. K., Basov, I. A., Scholl, D. W and Allan, J. F., 1995, Proceedings of the Ocean Drilling Program, Scientific Results, VOL 145, 1995.

Rea, D. K., Snoeckx, H. & Joseph, L. H. Late Cenozoic eolian deposition in the North Pacific: Asian drying, Tibetan uplift, and cooling of the northern hemisphere. *Paleoceanography* 13, 215–224, 1998.

Reece, R. S., Gulick, S. P. S., Horton, B. K., Christeson, G. L. and Worthington, L. L., Tectonic and climatic influence of the evolution of the Surveyor Fan and Channel system, Gulf of Alaska, Geosphere 7, 830-844, 2011.

Rosell-Melé, A., Carter, J. F., Parry, A. T. and Eglinton, G., *Determination of the UK37 Index in Geological Samples*, Analytical Chemistry, 67, 1283-1289, 1995.

Rodionov, S. N., Bond, N. A. and Overland, J. E., The Aleutian Low, storm tracks, and winter climate variability in the Bering Sea, Deep Sea Res., Part II, 54, 2560–2577, doi:10.1016/j.dsr2.2007.08.002, 2007.

Salzmann, U., Williams, M., Haywood, A. M. Johnson, A. I. A, Kender, S. and Zalasiewicz, J., Climate and environment of a Pliocene warm world, Palaeogeography, Palaeoclimatology, Palaeoecology, 309, 1-8, 2011.

Sánchez-Montes, M. L.; McClymont, E. L; Lloyd, J. M; Müller, J.; Cowan, E. A; Zorzi, C., Alkenone sea surface temperatures, ice rafted debris, terrestrial/aquatic n-alkane ratio, pollen counts and a new age and depth models from IODP Expedition 341 Site U1417, Gulf of Alaska. PANGAEA, 2019, https://doi.org/10.1594/PANGAEA.899064 (dataset in review).

Sarnthein, M., Schneider, B. and Grootes, P. M., Peak glacial ^{14}C ventilation ages suggest major draw-down of carbon into the abyssal ocean. Climate of the Past, 9, 2595-2614, 2013.

Schlitzer, R., Ocean Data View, odv.awi.de, 2018.

Seki, O., Foster, G. J., Schmidt, D. N., Mackensen, A., Kawamura, K. and Pancost, R. D., Alkenone and boron-based Pliocene pCO2 records, Earth and Planetary Science Letters 292, 201-211, doi:10.1016/j.epsl.2010.01.037, 2010.

Seki, Osamu; Foster, Gavin L; Schmidt, Daniela N; Mackensen, Andreas; Kawamura, Kimitaka; Pancost, Richard D, Alkenone and boron based Oligocene pCO2 records. PANGAEA, https://doi.org/10.1594/PANGAEA.732923, 2010. Supplement to: Seki, O., Foster, G. J., Schmidt, D. N., Mackensen, A., Kawamura, K. and Pancost, R. D.,Alkenone and boron based Pliocene pCO2 records. Earth and Planetary Science Letters, 292 (1-2), 201-211, https://doi.org/10.1016/j.epsl.2010.01.037, 2010.

Spies, R. B., *Long-term Ecological Change in the Northern Gulf of Alaska*, Elsevier, ISBN 978-0-444-52960-2, 2007.

St. John, K.E.K and Krissek, L.A., Regional patterns of Pleistocene ice-rafted debris flux in the North Pacific. Paleoceanography, Vol. 14, 653-662, 1999.

Swann, G. E. A., Snelling, A. M. and Pike, J., Biogeochemical cycling in the Bering Sea over the onset of major Northern Hemisphere Glaciation, Paleoceanography, 31, doi:10.1002/ 2016PA002978, 2016.

Tierney, J. E., and Tingley, M. P., BAYSPLINE: A new calibration for the alkenone paleothermometer. Paleoceanography and Paleoclimatology, 33, 281–301, 2018.

Zachos, J., M. Pagani, L. Sloan, E. Thomas, and K. Billups, Trends, rhythms, and aberrations in global climate 65 Ma to present,Science, 292(5517), 686–693, 2001a.

Walinsky, S.E., Prahl, F.G., Mix, A.C., Finney, B.P., Jaeger, J.M., and Rosen, G.P., *Distribution and composition of organic matter in surface sediments of coastal southeast Alaska*. Cont. Shelf Res., 29, 13, 1565–1579, doi:10.1016/j.csr.2009.04.006, 2009.

Weingartner, T., *Chapter 2.2: The physical environment of the Gulf of Alaska*. In: Spies, R.B. (Ed.), Long-term Ecological Change in the Northern Gulf of Alaska. Elsevier, Oxford, p. 589, 2007.

Weingartner, T, Danienlson, S., Shipton, P and Leech, D, *GAK 1 Time Series*, access online http://www.ims.uaf.edu/gak1/, last date accessed 23/12/2016, 2016.

Willeit, M., Ganopolski, A., Calov, R., Robinson, A. and Maslin, M., The role of CO_2 decline for the onset of Northern Hemisphere glaciation, Quaternary Science Reviews 119 (2015) 22e34, 2015.

5   **Table 1: Average SST (°C) and %$C_{37:4}$ during key climatic intervals 4.0-3.0 Ma, 3.0-2.8 Ma, 2.7-2.4 Ma, 2.4-1.7 Ma.** Average SST (°C) is the average of all the data points of the time interval, peak SST (°C) average is the average of the highest data points of each interval selected (Fig. 2), trough SST (°C) average is the average of the lowest data points of each interval (Fig. 5.2) and the average SST (°C) variability is the difference between average SST peak and the average SST trough. In black: data calculated from U^K_{37} (Prahl *et al*., 1988) and in black bold, data from U^K_{37}' (Müller *et al*., 1998).

Age intervals (Ma)	Average SST (°C)	Peak SST (°C) average	Trough SST (°C) average	Average SST variability (°C)	Average $C_{37:4}$ (%)	Peak $C_{37:4}$ (%)
4.0-3.1	10.2/**8.7**	12.5/**11.4**	7.2/**4.4**	5.3/**7.0**	1.9	10.5
3.1-2.8	8.5/**7.3**	9.9/**9.0**	7.4/**5.7**	2.4/**3.3**	3.9	4.9
2.7-2.4	10.2/**9.8**	13.2**12.6**	8.4/**6.6**	4.8/**5.9**	4.8	24.1
2.4-1.7	9.0/**8.6**	10.7/**10.4**	6.8/**4.8**	3.9/**5.6**	5.2	23.8
4-2.8 Ma	9.6/**8.2**	11.2/**10.2**	7.3/**5.1**	3.9/**5.2**	2.5	10.5
2.7-1.7Ma	9.6/**9.1**	12.0/**11.5**	7.6/**5.7**	4.4/**5.8**	5.0	24.1